Supporting Information (SI)

"Aggregation and Rebalance" Mechanism-Guided Design and Discovery of Efficient Bimetallic Catalysts for Nitrogen Reduction Reaction

[1] State Key Laboratory for Mechanical Behavior of Materials, School of Materials Science and Engineering, Xi'an Jiaotong University, Xi'an 710049, China
[2] School of Materials Science and Engineering, Chang'an University, Xi'an 710064, China

Table S1 Formation energies of different elements doped on substrates

TM_ATM_B elements	Formation energy (eV)
TiTi	-4.11
TiV	-3.32
TiCr	-3.23
TiMn	-3.29
TiFe	-2.39
TiCo	-2.75
TiNi	-3.25
TiMo	-2.86
TiW	-1.96
VV	-2.90
VCr	0.11
VMn	0.03
VFe	-1.89
VCo	-2.45
VNi	-0.68
VMo	-1.82
VW	-2.48
CrCr	-0.54
CrMn	-3.10
CrFe	-0.32
CrCo	-0.63
CrNi	-1.33
CrMo	-1.05
CrW	-1.73
MnMn	-1.57
MnFe	-1.06
MnCo	-1.45
MnNi	-2.02
MnMo	-0.25
MnW	-0.92
FeFe	-0.78
FeCo	-1.16
FeNi	-1.61
FeMo	-2.45
FeW	-1.75

CoCo	-3.45
CoNi	-3.67
CoMo	-3.13
CoW	-2.38
NiNi	-3.73
NiMo	-3.08
NiW	-2.38
MoMo	-2.02
MoW	-3.21
WW	-0.24

Table S2 Gibbs free energy changes for the first and last steps of hydrogenation

TM_A-TM_B elements	$G_{*N_2 \rightarrow *NNH}$ **(eV)**	$\Delta G_{*NH_2 \rightarrow *NH_3}$ **(eV)**
V-Cr	-0.30	0.44
V-Mn	0.38	-0.15
V-Ni	0.82	-0.67
V-Mo	0.26	-0.14
V-W	-0.22	0.36
Cr-Cr	-0.14	-0.25
Cr-Fe	0.21	-0.10
Cr-Co	0.59	-0.18
Cr-Ni	0.65	-0.83
Cr-Mo	-0.18	0.06
Cr-W	-0.14	0.34
Mn-Mn	0.23	0.12
Mn-Fe	0.26	-0.04
Mn-Co	0.33	-0.13
Mn-Ni	0.88	-0.54
Mn-Mo	0.24	-0.17
Mn-W	0.23	0.33
Fe-Fe	0.22	-0.24
Fe-Co	0.57	-0.25
Fe-Ni	0.33	-0.57
Mo-W	0.19	0.47

Table S3 The comparison of cohesion energy and binding energy for TM_A and TM_B atoms.

TM_A-TM_B elements	E_b (eV)	TM_A-E_c (eV)	TM_B-E_c (eV)
V-Cr	-9.63	-5.59	-4.15
V-Mn	-9.58	-5.59	-4.02
V-Ni	-11.66	-5.59	-5.39
V-Mo	-10.04	-5.59	-6.27
V-W	-11.53	-5.59	-8.42
Cr-Cr	-8.84	-4.15	-4.15
Cr-Fe	-9.96	-4.15	-5.49
Cr-Co	-10.41	-4.15	-5.63
Cr-Ni	-10.87	-4.15	-5.39
Cr-Mo	-9.37	-4.15	-6.27
Cr-W	-10.84	-4.15	-8.42
Mn-Mn	-9.61	-4.02	-4.02
Mn-Fe	-10.57	-4.02	-5.49
Mn-Co	-12.40	-4.02	-5.63
Mn-Ni	-11.43	-4.02	-5.39
Mn-Mo	-10.04	-4.02	-6.27
Mn-W	-11.52	-4.02	-8.42
Fe-Fe	-11.76	-5.49	-5.49
Fe-Co	-12.28	-5.49	-5.63
Fe-Ni	-12.49	-5.49	-5.39
Mo-W	-11.48	-6.27	-8.42

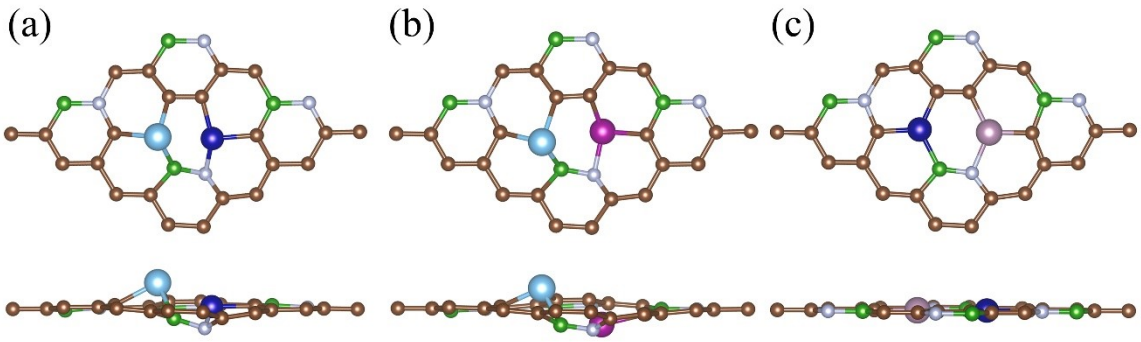

Fig. S1. Scheme of the structures of $TM_ATM_B@BC_6N$ nanosheets undergoing different degrees of deformation.

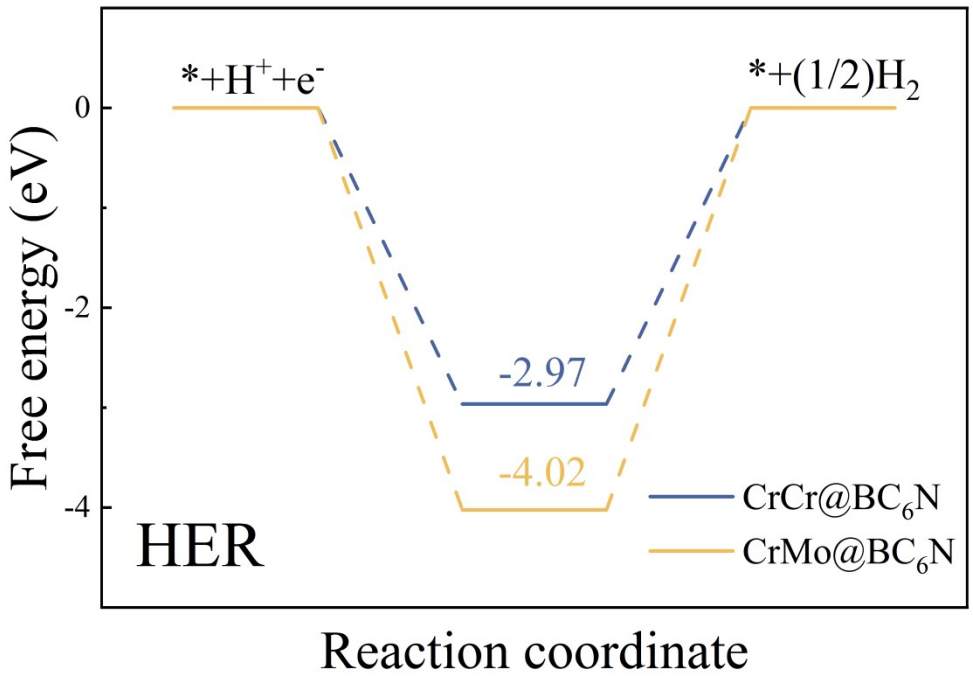

Fig. S2. Gibbs free energy diagram of HER for CrCr@BC_6N and CrMo@BC_6N nanosheets.

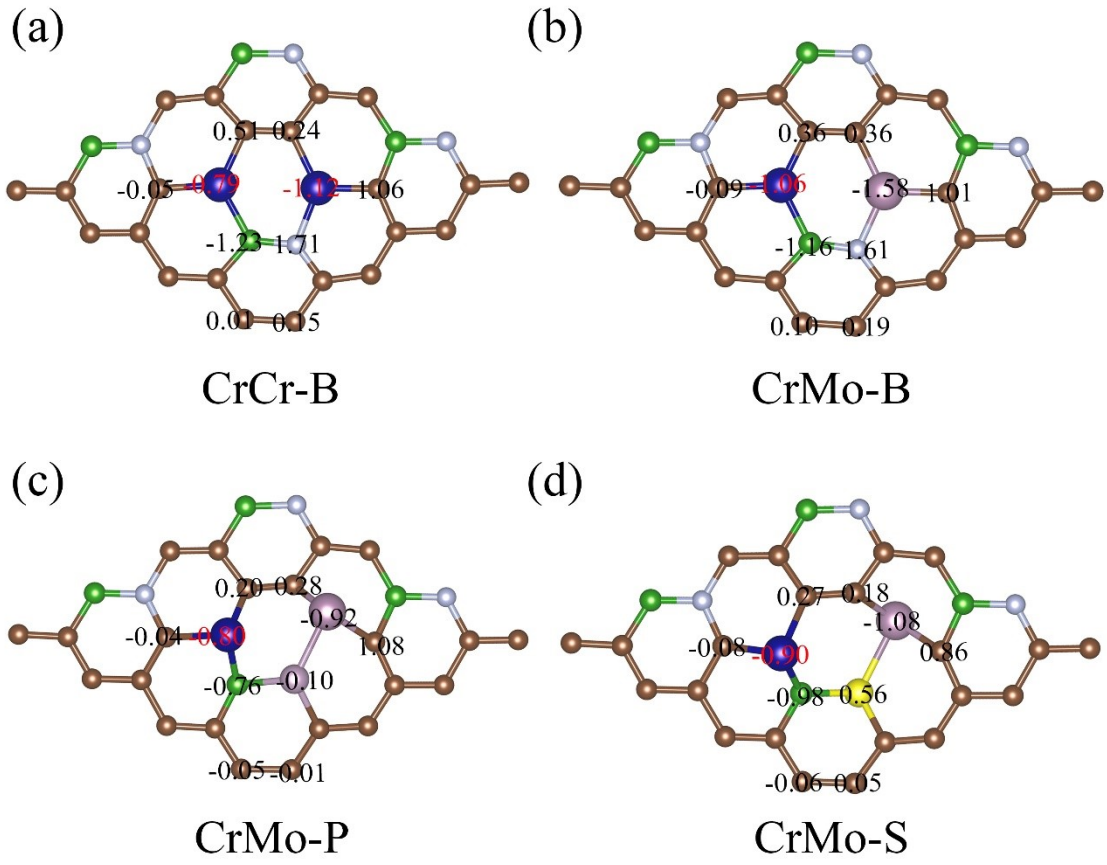

Fig. S3. Changes in charge of active centre atoms and coordination atoms for (a) CrCr@BC_6N, (b) CrMo@BC_6N, (c,d) CrMo@BC_6N with coordination d N atom replaced with P and S atom.

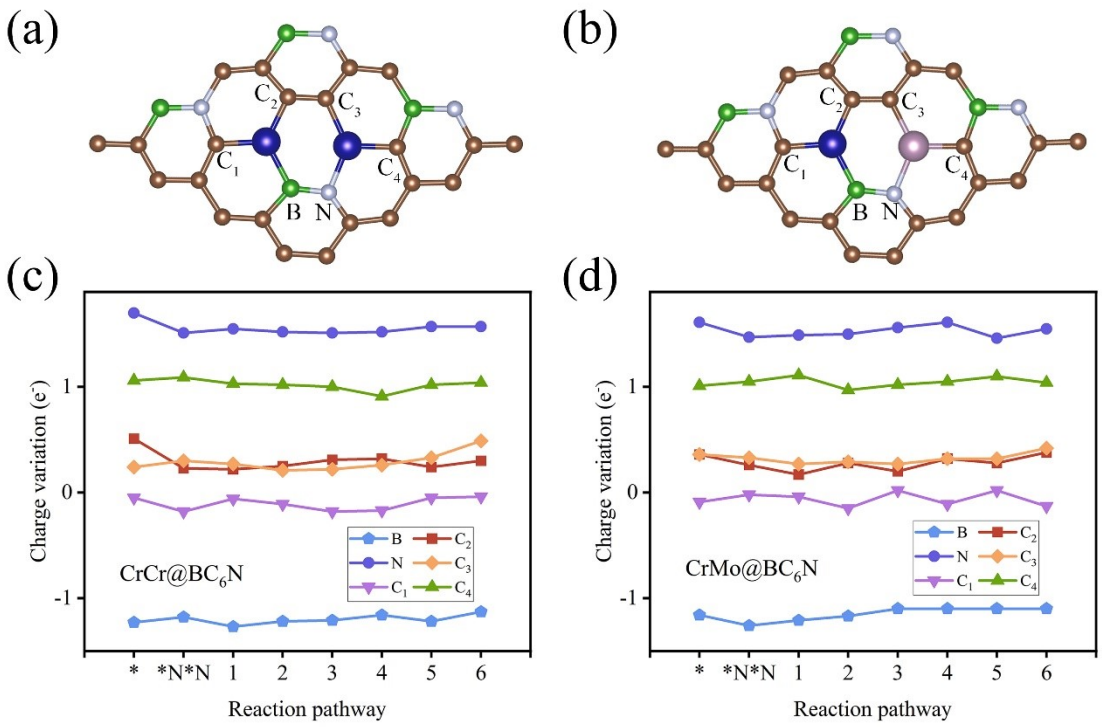

Fig. S4. Charge fluctuations of 6 coordinating atoms for NRR on $CrCr@BC_6N$ and $CrMo@BC_6N$.

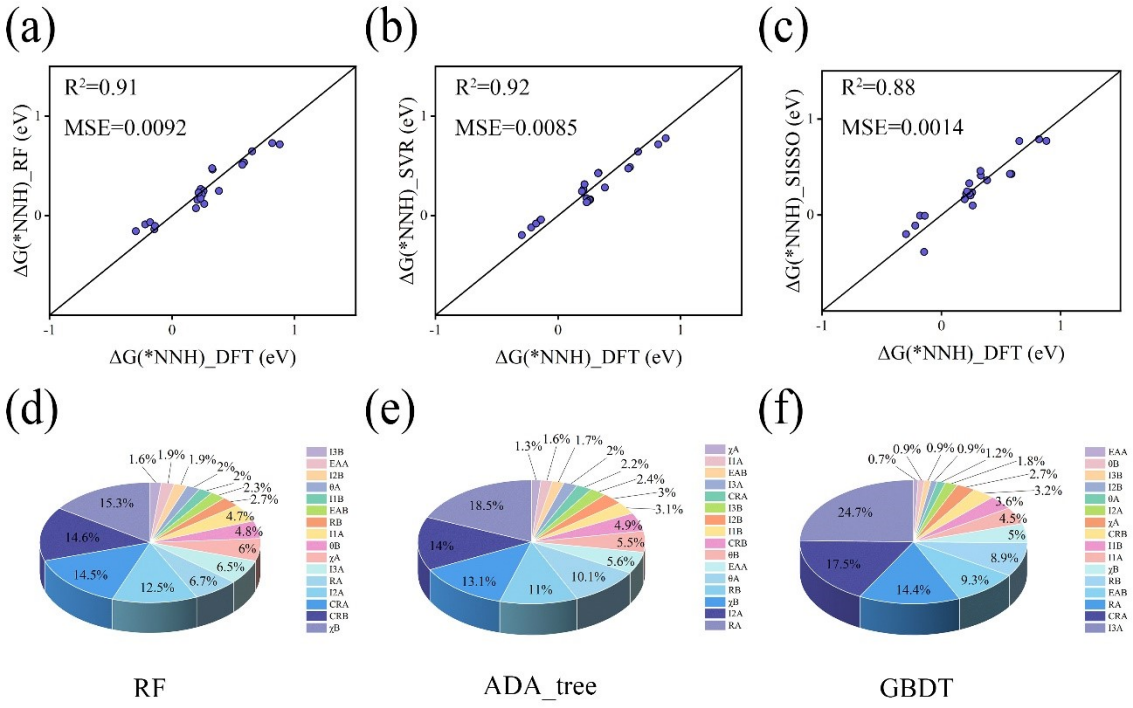

Fig. S5. Machine learning training and importance analysis of $^{\Delta G}{}_{*NNH}$ under different algorithmic models.

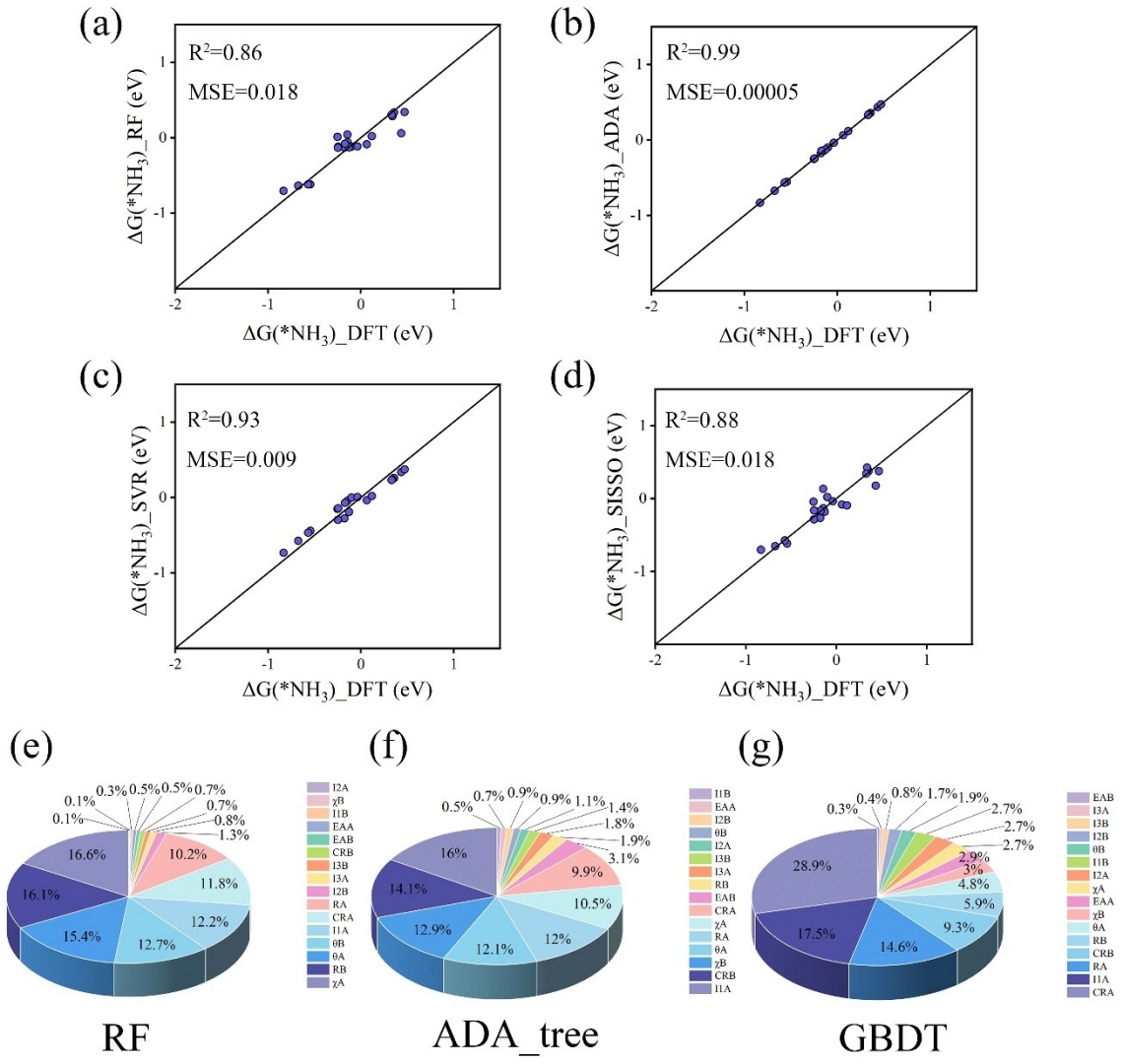

Fig. S6. Machine learning training and importance analysis of ΔG_{*NH_3} under different algorithmic models.

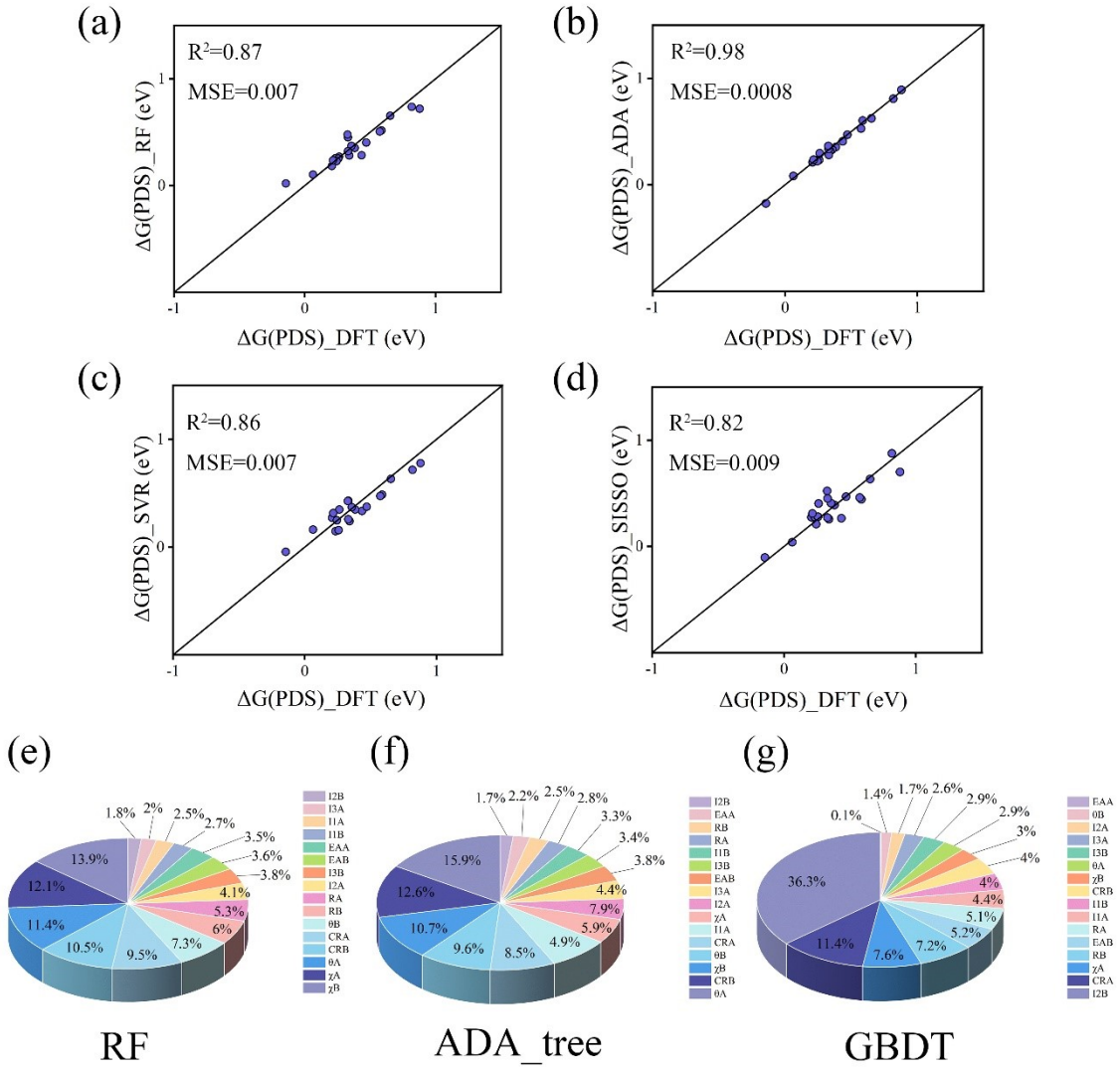

Fig. S7. Machine learning training and importance analysis of ΔG_{PDS} under different algorithmic models.

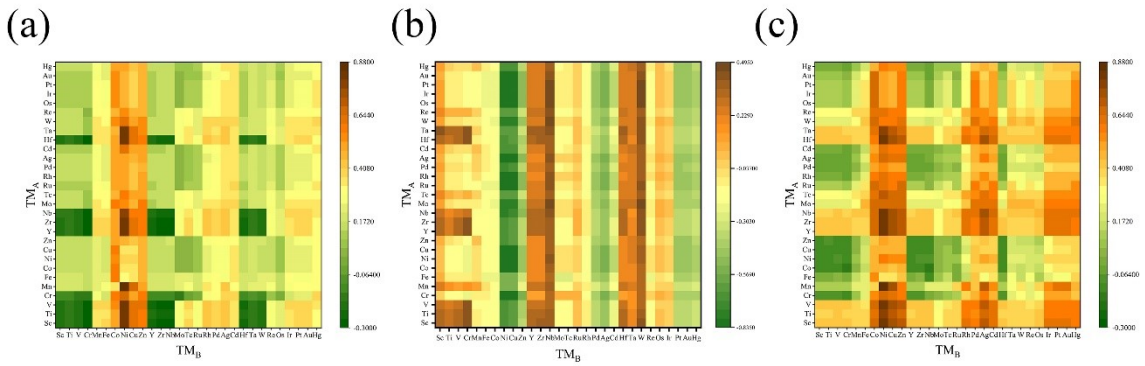

Fig. S8. Results of predictions for 842 structures using the GBDT algorithm for (a) ΔG_{*NNH}, (b) ΔG_{*NH_3}, (c) ΔG_{PDS}.

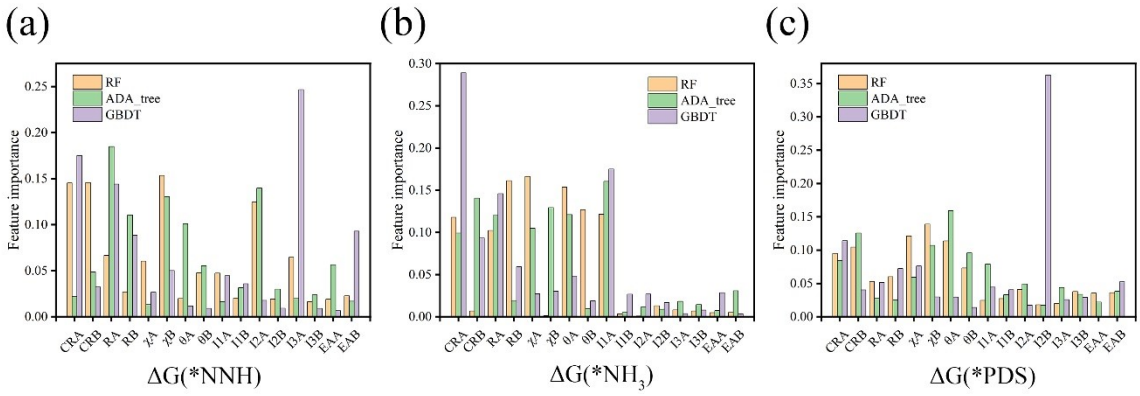

Fig. S9. Comparison of the feature importance of the three algorithms for each of the three datasets, ΔG_{*NNH}, ΔG_{*NH_3}, and ΔG_{PDS}.

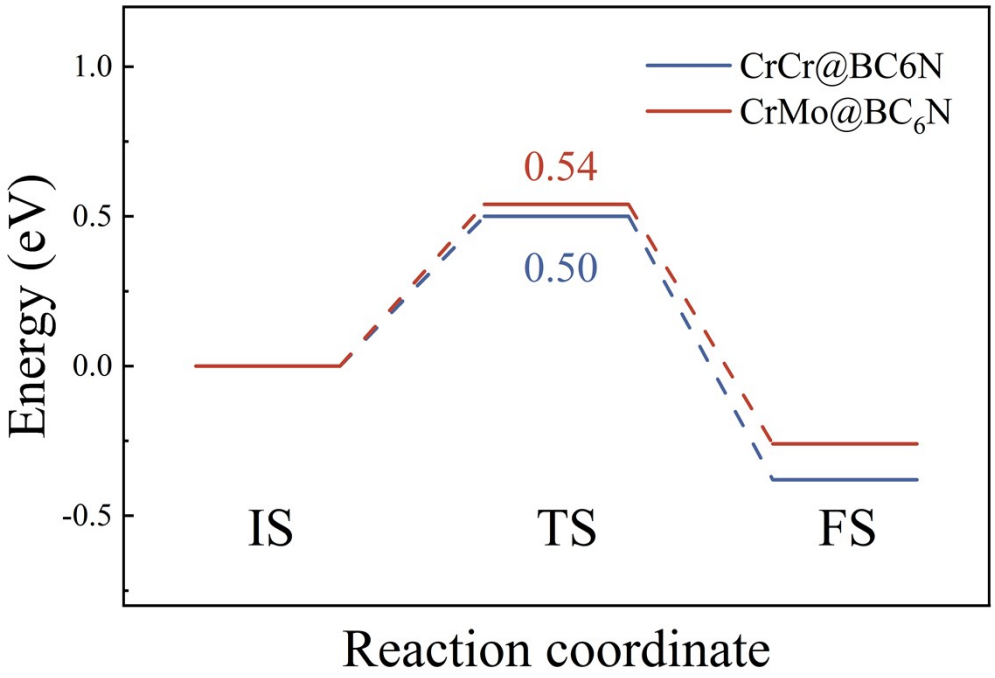

Fig. S10. The energy barrier of the PDS for nitrogen reduction reaction catalyzed by $CrCr@BC_6N$ and $CrMo@BC_6N$.

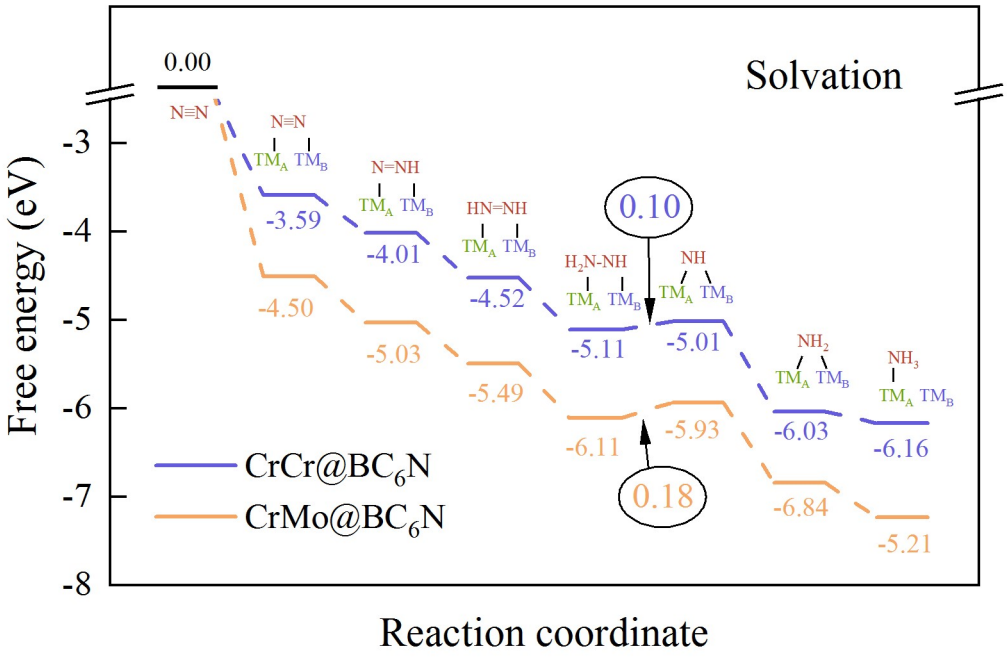

Fig. S11. Free energies of the optimal NRR pathway in the solvation model for $CrCr@BC_6N$ and $CrMo@BC_6N$.

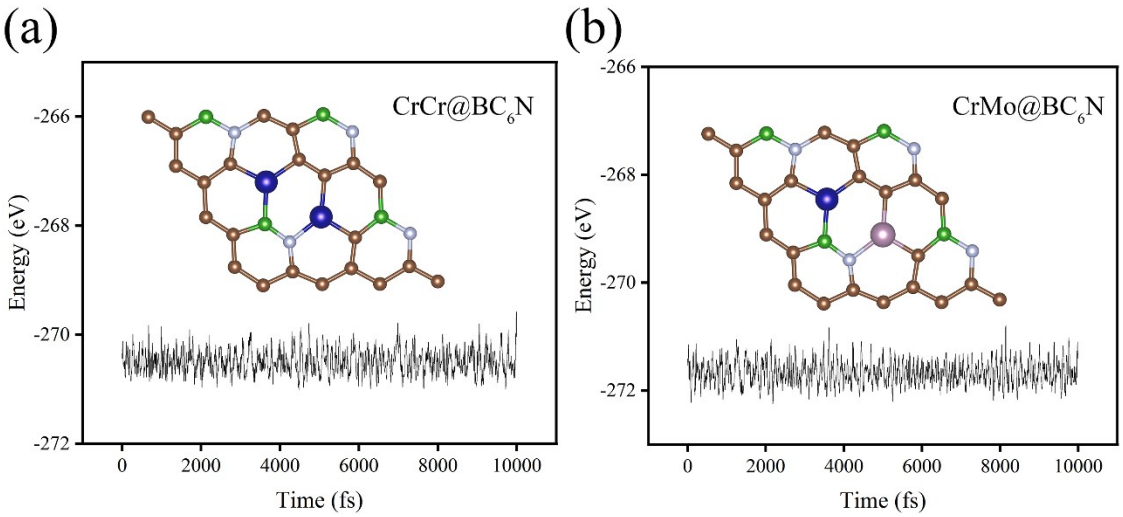

Fig. S12. The MD simulation for $CrCr@BC_6N$ and $CrMo@BC_6N$ under 298.15 K.